

# THE BUTTERFLY EFFECT IN THE EXTREME-MASS RATIO INSPIRAL PROBLEM

PAU AMARO-SEOANE<sup>1,2</sup>, PATRICK BREM<sup>3</sup>, JORGE CUADRA<sup>4</sup> & PHILIP J. ARMITAGE<sup>5</sup>

(Dated: December 15, 2011)  
Draft version December 15, 2011

## ABSTRACT

Measurements of gravitational waves from the inspiral of a stellar-mass compact object into a massive black hole are unique probes to test General Relativity (GR) and MBH properties, as well as the stellar distribution about these holes in galactic nuclei. Current data analysis techniques can provide us with parameter estimation with very narrow errors. However, an EMRI is not a two-body problem, since other stellar bodies orbiting nearby will influence the capture orbit. Any deviation from the isolated inspiral will induce a small, though observable deviation from the idealised waveform which could be misinterpreted as a failure of GR. Based on conservative analysis of mass segregation in a Milky Way like nucleus, we estimate that the possibility that another star has a semi-major axis comparable to that of the EMRI is non-negligible, although probably very small. This star introduces an observable perturbation in the orbit in the case in which we consider only loss of energy via gravitational radiation. When considering the two first-order non-dissipative post-Newtonian contributions (the periastron shift of the orbit), the evolution of the orbital elements of the EMRI turns out to be chaotic in nature. The implications of this study are twofold. From the one side, the application to testing GR and measuring MBHs parameters with the detection of EMRIs in galactic nuclei with a millihertz mission will be even more challenging than believed. From the other side, this behaviour could in principle be used as a signature of mass segregation in galactic nuclei.

## 1. MOTIVATION

A stellar mass black hole or neutron star executes  $\sim 10^{5-6}$  orbits during the final year of inspiral toward a  $\sim 10^6 M_\odot$  supermassive black hole (MBH). The large number of cycles implies that a phase-coherent measurement of the inspiral, achievable through detection of low frequency gravitational waves, would be a tremendously powerful probe of the space-time near a black hole (Amaro-Seoane et al. 2007; Hughes 2009). Among other things, it would enable a precise determination of the spin of the supermassive black hole, and a test of General Relativity that is independent of current constraints derived from pulsar timing data.

There is no foreseeable instrument sensitive enough to detect gravitational waves from extreme mass ratio inspirals (EMRIs) over time scales comparable to the orbital period. As a consequence, realizing the astrophysical and gravitational physics promise of EMRIs requires an assurance that the inspiral can be accurately modeled over many orbits using templates calculated by solving the 2-body problem in General Relativity (for a review, see e.g., Barack 2009). It is therefore necessary to assess whether gas, stars or other compact objects in the vicinity, could significantly perturb EMRI trajectories. In the case of gas, perturbations to stellar mass black holes or neutron stars<sup>6</sup> are securely negligible provided that

accretion on to the black hole occurs in a low density, radiatively inefficient flow (Narayan 2000). Such flows are much more common than dense accretion discs, which *would* yield observable phase shifts during inspiral (Kocsis et al. 2011), at least at the relatively low redshifts where EMRIs may be observed.

In this Letter, we quantify the nature and strength of possible perturbations from point mass perturbers: low mass stars or compact objects in tight orbits around the supermassive black hole. Any perturbers are unlikely to orbit close enough to the EMRI to undergo strong interactions, so the regime of interest is one where the third body is relatively distant and the interaction weak. The Newtonian analog of this problem has been studied extensively in the context both of Solar System satellite evolution, and for transit timing variations of extra-solar planets (Dermott, Malhotra & Murray 1988; Agol et al. 2005; Holman & Murray 2005; Veras, Ford & Payne 2011). In Newtonian gravity, perturbations are strong only at the location of mean motion resonances, and these have the effect of inducing small jumps in eccentricity upon divergent resonance crossing. This would already be interesting for the EMRI problem, since the jumps in eccentricity would result in a perturbation to the gravitational wave decay rate, and an eventual dephasing of the waveform. However, as we will see, the inclusion of post-Newtonian corrections changes the evolution qualitatively. Computing trajectories that include the two first-order non-dissipative post-Newtonian corrections, we find evidence of dependence on initial conditions in the evolution of the perturbed inner binary, such that arbitrarily small variations in the initial orbit lead to significantly different future behaviour.

## 2. ASTROPHYSICAL LIMITS ON PERTURBERS

Is it likely that a star or compact object will be present close enough to perturb the orbit of an EMRI? Excluding low mass MBHs ( $M_* < 10^6 M_\odot$ ), where the stellar tidal disruption limit comes into play, the existence of perturbers is not excluded by

<sup>1</sup> Max Planck Institut für Gravitationsphysik (Albert-Einstein-Institut), D-14476 Potsdam, Germany

<sup>2</sup> Institut de Ciències de l'Espai (CSIC-IEEC), Campus UAB, Torre C-5, parells, 2<sup>na</sup> planta, ES-08193, Bellaterra, Barcelona, Spain

<sup>3</sup> Astronomisches Rechen-Institut, Mönchhofstraße 12-14, 69120, Zentrum für Astronomie, Universität Heidelberg, Germany

<sup>4</sup> Departamento de Astronomía y Astrofísica, Pontificia Universidad Católica de Chile, Santiago, Chile

<sup>5</sup> JILA, University of Colorado and NIST, at Boulder, 440 UCB, Boulder, CO 80309-0440, USA

<sup>6</sup> White dwarf EMRIs are excluded here, because mass loss from the compact object itself could form a dynamically significant disc even if the background accretion flow is of low density (Zalamea, Menou & Beloborodov 2010).

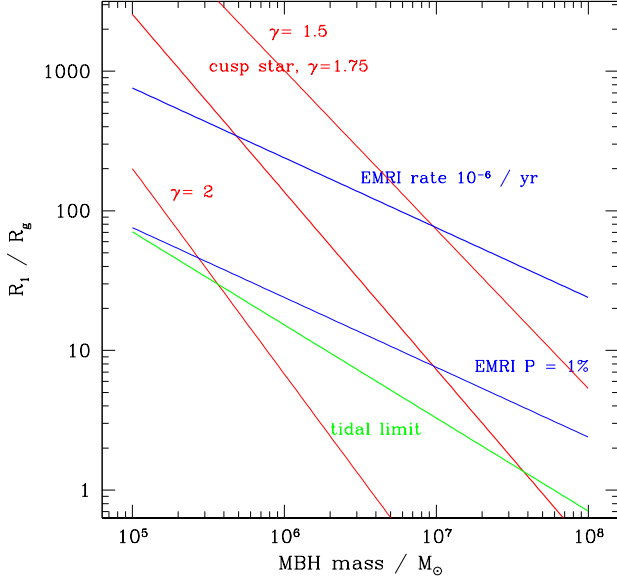


FIG. 1.— Estimates for the semi-major axis of the innermost perturbing body around a massive black hole, scaled to the hole’s gravitational radius  $R_g = GM_\bullet/c^2$ . The red lines show the location of the innermost star, estimated assuming that stars of mass  $0.3 M_\odot$  follow a single power-law cusp of index  $\gamma$  in a galaxy on the  $M_\bullet$ - $\sigma$  relation. The green line shows the tidal disruption limit for such stars. The blue lines show the average (upper) and 1% probability (lower) location of the next nearest EMRI, assuming uncorrelated inspirals at a rate of  $10^{-6} \text{ yr}^{-1}$ .

elementary arguments. Neither, however, is it easy to calculate the probability distribution of perturbers, whose proximity will depend upon the details of discreteness and relativistic effects very close to the MBH, and mass segregation and EMRI injection mechanisms in galactic nuclei (Preto et al. 2004; Freitag et al. 2006; Amaro-Seoane et al. 2004).

Rather than face these difficulties, we limit ourselves here to order of magnitude estimates for the likely location of the nearest star and compact object. For stars, assumed to be of a single mass  $M_*$ , we assume a cusp-like distribution with density profile  $\rho \propto R^{-\gamma}$ , extending from the MBH to its radius of influence  $R_{\text{BH}} = GM_\bullet/\sigma^2$ . Here  $\sigma$  is the velocity dispersion of the galaxy. Using the fact that the enclosed mass,  $M(R) \simeq M_\bullet$  at  $R = R_{\text{BH}}$ , we find that the expected radius of the innermost star,  $R_1$ , is,

$$\frac{R_1}{R_g} = \left( \frac{M_*}{M_\bullet} \right)^{1/(3-\gamma)} \left( \frac{c}{\sigma} \right)^2, \quad (1)$$

where  $R_g = GM_\bullet/c^2$ . This formula yields an explicit estimate for  $R_1$  once we adopt a relation between  $M_\bullet$  and  $\sigma$  (Gültekin et al. 2009). For the location of the next nearest compact object (or EMRI), we use an even simpler approach. We calculate the expected semi-major axis for uncorrelated inspirals due to gravitational radiation (Peters 1964), assuming near-circular orbits and rate  $\dot{N}_{\text{EMRI}}$ . Finally, we plot the tidal limit (e.g. Rees 1988) for  $0.3 M_\odot$  main-sequence stars.

Figure 1 shows these estimates as a function of  $M_\bullet$ . For a standard cusp slope  $\gamma = 1.75$ , there is likely to be a low mass stellar perturber within a few hundred  $R_g$  for  $M_\bullet > 10^6 M_\odot$ . Similarly, if the EMRI rate is as high as  $10^{-6} \text{ yr}^{-1}$ , there is a significant chance (at least a few percent) that a second compact object will be present between  $10 - 10^2 R_g$  for

$10^6 M_\odot < M_\bullet < 10^7 M_\odot$ . Clearly, these crude estimates do not demonstrate that *most* EMRIs will be perturbed by third bodies, but they do suggest that perturbers may be close enough in some galaxies to motivate detailed consideration of their dynamical effects.

### 3. METHODS

We are interested in the secular effect of a star acting on an EMRI which will describe thousands of orbits in the detector bandwidth and slowly decay. The kind of effects on the wave that we are looking at are tiny, though detectable, and the mass difference between the two binaries (the MBH-EMRI and the MBH-star systems) is huge. We need therefore a numerical tool capable of integrating the plunging orbit of the EMRI while inducing a minimal error in the integration, since data analysis techniques can detect e.g. eccentricity differences of the order  $\Delta e \sim 10^{-3}$  (Amaro-Seoane et al. 2010; Porter & Sesana 2010; Key & Cornish 2011). We hence have chosen to use a direct  $N$ -body approach (Aarseth 1999, 2003), the planet code, written by Aarseth<sup>7</sup>. This is the most expensive method because it involves integrating all gravitational forces for all three bodies at every time step, without making any a priori assumptions about the system. Our approach employs the improved Hermite integration scheme, which requires computation of not only the accelerations but also their time derivatives. Since we are simply integrating Newton’s equations directly, all gravitational effects are included. For the purpose of our study, nonetheless, we have included relativistic corrections to the Newtonian forces (the forces can be found in the same page in the `toy` code<sup>8</sup>). This was first implemented in a direct-summation  $N$ -body code by Kupi et al. (2006). For this, one has to add perturbations in the integration, so that the forces are modified by

$$F = \underbrace{F_0}_{\text{Newt.}} + \underbrace{c^{-2}F_2 + c^{-4}F_4}_{\substack{\text{1PN} \quad \text{2PN}}} + \underbrace{c^{-5}F_5}_{\text{2.5PN}} + \underbrace{\mathcal{O}(c^{-6})}_{\text{neglected}} \quad (2)$$

In the last equation “PN” stands for post-Newtonian. We note that the perturbations do not need to be small compared to the two-body force (Mikkola 1997). The expressions for  $F_2$ ,  $F_4$  and  $F_5$  can be found in Blanchet & Faye (2001), their equation 7.16.

### 4. DISSIPATION OF ENERGY AND RESONANCES

We first analyse the system by contemplating only the relativistic effect of dissipation of energy; i.e. our simulations only incorporate the 2.5 PN correction term. We stop the integration when the separation between the stellar BH and the MBH is  $a_\bullet = 5 R_{\text{Schw}}$ , which approximately corresponds to the limit where the PN approximation is not valid anymore. The inspiral down to this distance takes typically in our simulations some 440,000 orbits.

In Fig.(2) the test stellar black hole of mass  $m_\bullet = 10 M_\odot$  has been initially set in such an orbit that it is totally embedded in a LISA-like detector band (i.e. with an orbital period  $< 10^5$  secs, namely  $P_\bullet = 6 \times 10^3$  secs) and is hence an EMRI; its initial semi-major axis is  $a_{\bullet,i} \simeq 1.45 \times 10^{-6} \text{ pc}$  and its eccentricity  $e_{\bullet,i} = 0.05$ . The perturber, a star of mass  $m_* = 10 M_\odot$  is

<sup>7</sup> who, as is his admirable custom, has made the code publicly available <http://www.ast.cam.ac.uk/~sverre/web/pages/nbody.htm>

<sup>8</sup> <ftp://ftp.ast.cam.ac.uk/pub/sverre/toy/README>

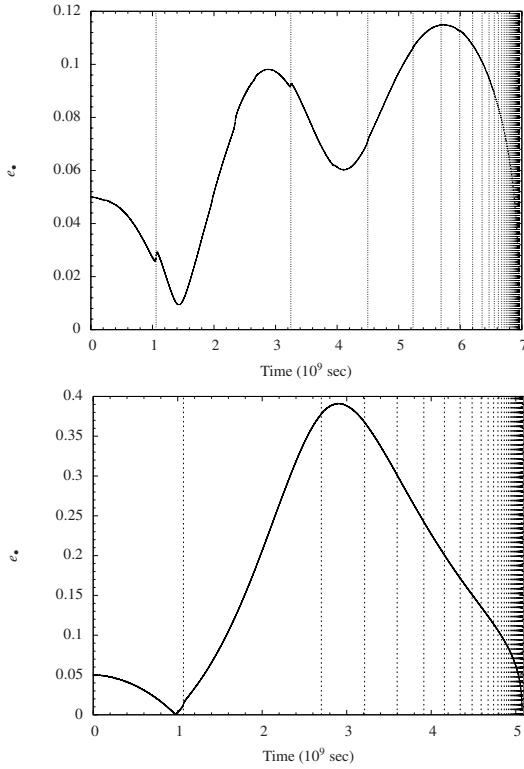


FIG. 2.— *Upper panel:* Results for the fiducial case using the direct-summation  $N$ -body integrator. The mass of the MBH is  $\mathcal{M}_\bullet = 10^6 M_\odot$ , the mass of the stellar black hole is  $m_\bullet = 10 M_\odot$ . See text for more details. *Lower panel:* Same configuration but with an initial inclination of the star of  $i_* = 45^\circ$  instead of  $30^\circ$ , i.e. the inclination triggers the Kozai mechanism, since  $i_* > 39.2^\circ$  and the orbit is prograde. As mentioned in the previous case, even if the changes in eccentricity cannot be directly seen in the curve, they are of the order  $\Delta e_\bullet \sim 10^{-3}$ .

initially on an orbit in which the semi-major axis has the value  $a_{*,i} \simeq 4.1 \times 10^{-6}$  pc and the eccentricity at  $T = 0$  is  $e_{*,i} = 0.5$ . The inclination of the system EMRI – star was set to  $30^\circ$  initially in the upper panel. This constitutes our reference system.

In the figure, the straight lines mark the condition  $P_*/P_\bullet = A$ , with  $A$  an integer,  $P_*$  the period of the star around the MBH and  $P_\bullet$  the period of the EMRI around the MBH; i.e. where the resonances occur. The first three resonances have an impact on  $e_\bullet$  which can be seen on the plot; later resonances do also affect  $e_\bullet$ , with  $\Delta e_\bullet \sim 10^{-3}$ . We also note that in the upper panel one can see in-between smaller jumps; they correspond to higher-order resonances,  $P_*/P_\bullet = 5.5, 6.5$  and  $7.5$ .

We made the choice for an initial inclination of  $30^\circ$  to avoid another effect that introduces a change in the eccentricity. In the lower panel we have *exactly* the same system but for  $i_* = 45^\circ$ . With this value, and the fact that the orbit is prograde, the Kozai oscillation of eccentricity is present (Kozai 1962). Even if the eccentricity of the EMRI  $e_\bullet$  suffers the characteristic Kozai oscillations, the loci for the resonances still fulfill the condition  $P_*/P_\bullet = \text{integer}$ .

##### 5. DOES THE FLAP OF THE STAR AT APOAPSIS SET OFF A TORNADO AT PERIAPSIS?

In this subsection we address numerically the effect of including the relativistic periastron shift along with the dissipation of energy; i.e. the set of corrections as specified in Eq.(2). As we show below, the effect of the periastron shift changes completely the evolution of the system. In Fig.(3) we show

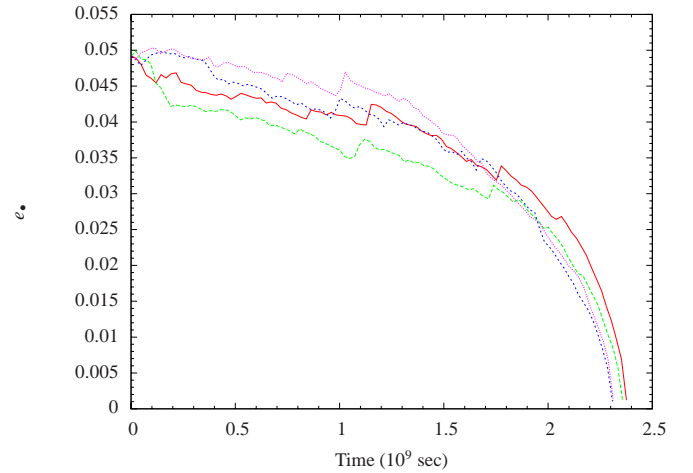


FIG. 3.— Fiducial case with energy dissipation and periastron shift correcting terms for different initial inclinations of the perturber. The solid (red) curve corresponds to  $i_* = 30^\circ$ , the long-dashed (green) to  $i_* = 30.001^\circ$ , the short-dashed (blue) corresponds to the fiducial case plus a *billionth* of a degree,  $i_* = 30.0000000001^\circ$  and the dotted (magenta) to the reference plus a  $10^{-13}$  of a degree,  $i_* = 30.000000000001^\circ$ .

four cases. One of them corresponds to the reference system but taking into account the periastron shift. We only display these examples but note that the behaviour is also chaotic<sup>9</sup> for other nearby choices of  $i_*$ . When using an initial inclination of  $i_* = 45^\circ$ , which corresponds to the same situation as in the lower panel of Fig.(2) but taking into account the periastron shift, along with another case which is identical but for  $i_* = 45.0000000001^\circ$ , we find also a chaotic result which moreover eliminates the secular Kozai oscillation of  $e$ .

We have systematically studied this chaotic behaviour by running hundreds of simulations in which we methodically increase in minimal differences an initial dynamical orbital parameter such as the inclination, semi-major axis or eccentricity. In all cases and parameters the evolution corroborates the chaotic behaviour of the system. We have also tested a mass for the perturbing star of 5 and  $1.44 M_\odot$ , as well as different values of  $e_*$  (0.1, 0.3, 0.7 and 0.9), with similar results.

In order to fence in the region within which the system is chaotic, we systematically increase the semi-major axis of the star and run the same experiment. We start with the same difference in inclination at a slightly larger semi-major axis, and then regularly increase it until we reach one order of magnitude over the fiducial case, as we depict in Fig.(4). The chaotic behaviour ceases at about one order of magnitude of the initial value of  $a_*$  in the reference case.

##### 6. QUANTIFYING THE DEPENDENCE ON INITIAL CONDITIONS OF THE SYSTEM

In this section we present a way of characterizing the rate of separation of infinitesimally close trajectories systematically. To achieve this we compare our fiducial model with another case in which we set up the EMRI in an (almost) imperceptibly different initial orbit (the initial difference is  $2 \times 10^{-10}$  pc, while the objects are moving on the same ellipse) and keep the same initial conditions of the MBH and the perturber. Hence EMRI in the second case differs only from the reference case slightly and has an initial distance separation of  $r_0$ . We say that the two models are in phase provided that

<sup>9</sup> When we use the word, we do not follow the rigorous mathematical definition of chaos. We mean a strong dependence on the initial conditions.

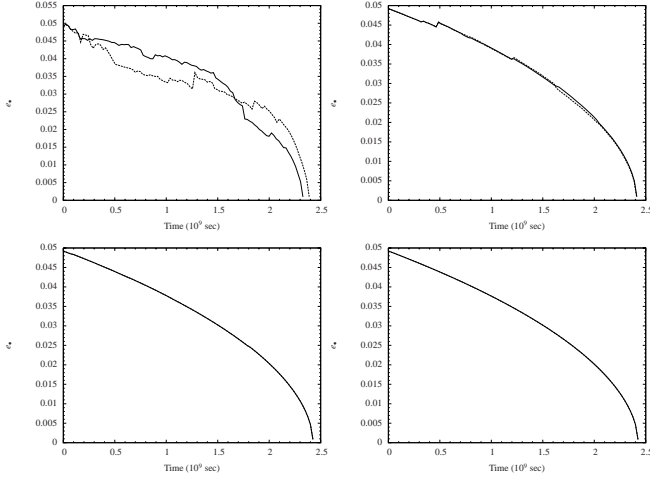


FIG. 4.— Same as in Fig.(3) but we set initially the perturber at a larger and larger initial semi-major axis. From the top to bottom and from the left to the right, the semi-major axis of the perturber is  $a_* = 4 \times 10^{-6}$  pc,  $6 \times 10^{-6}$  pc,  $9 \times 10^{-6}$  pc and  $4.07243 \times 10^{-5}$  pc. Solid lines correspond to  $i_* = 30^\circ$  and dashed lines to  $i_* = 30.0000000001^\circ$ .

$$r \approx r_0. \quad (3)$$

If the two different realizations reach a separation

$$r \approx 2a_*. \quad (4)$$

the EMRI bodies are moving out of phase, on entirely unrelated orbits. We thence are able to estimate a characteristic timescale  $\tau_{\text{deph}}$  for the system to become out of phase. In Fig.(5) we display the separation of the two systems for different distances to the perturber. From these figures we can measure the value of a characteristic timescale  $\tau_{\text{deph}}$  for a given  $a_*$ .

From the data points obtained in the upper panels of Fig.(5) we can then derive the relation displayed in the lower panel. For large enough distances, of the order of  $\sim 10^{-5}$  pc the two timescales converge and the system becomes deterministic.

## 7. CONCLUSIONS

In this paper we have addressed the role of a perturbation on an EMRI by a nearby star. The system depends extremely on *minimal* changes in the initial conditions (as small as a  $10^{-9}$  part in the inclination) lead to a very different dynamical evolution. In all cases, however, the Kozai mechanism is washed out by the periastris shift, as one can expect (see e.g. Holman et al. 1997; Blaes et al. 2002). For distances of the order of  $a_* \sim 10^{-5}$  pc the system enters the chaotic regime, for perturbing masses as small as  $1.44 M_\odot$ . While we cannot state clearly whether this will be a common feature for EMRIs, since the different dynamical and relativistic phenomena involved in the problem are many and not straightforward (see for a review Amaro-Seoane et al. 2007 and also Amaro-Seoane 2011 for a dedicated review of the dynamics), it seems plausible that for a Milky Way-like galaxy a star can

be at such a radius from the EMRI system that it will significantly perturb it. From the standpoint of detection and data analysis, this is yet another complication of the problem and could even lead to the misinterpretation that nature's GR is not what we believe it to be. On the other hand, from the point of view of stellar dynamics, the detection of one of these systems would shed light on our current understanding of galactic dynamics in general and mass segregation in particular.

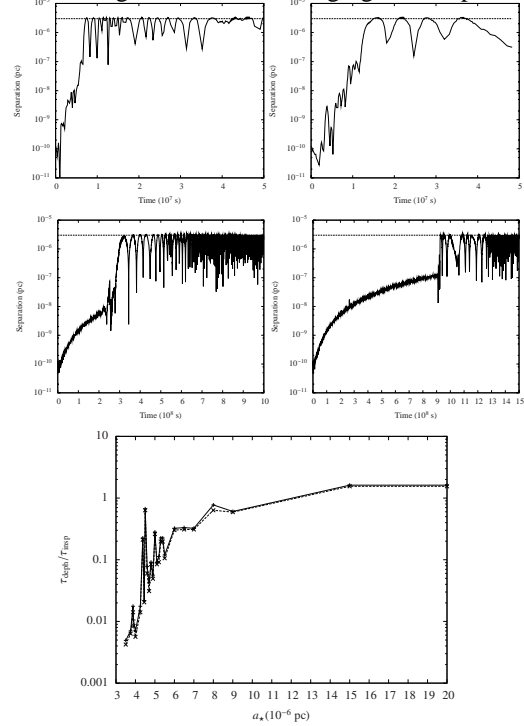


FIG. 5.— *Upper panels:* From the left to the right and from the top to the bottom we show the separation  $r$  for a increasing separation of the perturbing star of  $3.5 \times 10^{-6}$ ,  $3.9 \times 10^{-6}$ ,  $4.375 \times 10^{-6}$ , and  $4.5 \times 10^{-6}$  pc. The dashed line shows the critical distance  $2a_*$ . Note the different timescales in the lower panels. *Lower panel:*  $\tau_{\text{deph}}$  against distance to the perturber normalized to the gravitational radiation timescale of the isolated system  $\tau_{\text{insp}}$ ; i.e. the merger timescale without the perturber acting onto the binary MBH-EMRI.

We thank Marc Freitag and Rainer Schödel for comments on the manuscript. PJA acknowledges support from the NSF (AST-0807471), from NASA's Origins of Solar Systems program (NNX09AB90G), and from NASA's Astrophysics Theory program (NNX11AE12G). PAS and JC were supported in part by the National Science Foundation under Grant No. 1066293 and thank the hospitality of the Aspen Center for Physics. JC acknowledges support from FONDAP (15010003), FONDECYT (11100240), Basal (PFB0609) and VRI-PUC (Inicio 16/2010), and the hospitality of JILA, AEI and MPE. PB and PAS acknowledge financial support for research visits in China by The Silk Road Project (2009S1-5) of Chinese Academy of Sciences, National Astronomical Observatories of China and PB also the University of Heidelberg for travel costs through the excellence initiative ZUK 49/1, TP 14.8 International Research. It is a pleasure for PAS to thank Sabine Pendl for her extraordinary support at the Rote Insel during the preparation of this work and also for her interest in non-linear dynamics and complex systems, which motivated very interesting discussions.

## REFERENCES

- Aarseth, S. J. 1999, The Publications of the Astronomical Society of the Pacific, 111
- . 2003, Gravitational N-Body Simulations (ISBN 0521432723. Cambridge, UK: Cambridge University Press, November 2003.)

- Agol E., Steffen J., Sari R., Clarkson W., 2005, MNRAS, 359, 567
- Amaro-Seoane, P., Freitag, M., & Spurzem, R. 2004, MNRAS
- Amaro-Seoane P., Gair J. R., Freitag M., Miller M. C., Mandel I., Cutler C. J., Babak S., 2007, Classical and Quantum Gravity, Vol. 24, Issue 17, R113
- Amaro-Seoane P., 2011 Living Reviews in Relativity (to be submitted soon)
- Amaro-Seoane, P., Eichhorn, C., Porter, E. K., & Spurzem, R. 2010, MNRAS, 401, 2268
- Amaro-Seoane, P., & Preto, M. 2011, Classical and Quantum Gravity, 28, 094017
- Barack L., 2009, Classical and Quantum Gravity, Vol. 26, Issue 21, pp. 213001
- Blaes, O., Lee, M. H., & Socrates, A. 2002, ApJ, 578, 775
- Blanchet, L., & Faye, G. 2001, Phys. Rev. D, 63, 062005
- Dermott S. F., Malhotra R., Murray C. D., 1988, Icarus, 76, 295
- Freitag, M., Amaro-Seoane, P., & Kalogera, V. 2006, ApJ, 649, 91
- Ghez, A. M. et al. 2008, ApJ, 689, 1044
- Gültekin K., et al., 2009, ApJ, 698, 198
- Holman M. J., Murray N. W., 2005, Science, 307, 1288
- Holman, M., Touma, J., & Tremaine, S. 1997, Nature, 386
- Hughes S. A., 2009, ARA&A, 47, 107
- Key, J. S., & Cornish, N. J. 2011, Phys Rev D, 83
- Kocsis, B., Yunes, N., & Loeb, A. 2011, Phys. Rev. D, 84, 024032
- Kozai, Y. 1962, AJ, 67
- Kupi, G., Amaro-Seoane, P., & Spurzem, R. 2006, MNRAS, L77+
- Mikkola, S. 1997, Celestial Mechanics and Dynamical Astronomy, 68
- Narayan R., 2000, ApJ, 536, 663
- Peters P. C., 1964, Physical Review, 136, 1224
- Porter, E. K., & Sesana, A. 2010, ArXiv e-prints, arXiv:1005.5296
- Preto, M., Merritt, D., & Spurzem, R. 2004, ApJ Lett., 613
- Preto, M., & Amaro-Seoane, P. 2010, ApJ Lett., 708, L42
- Rees, M. J. 1988, Nature, 333, 523
- Veras D., Ford E. B., Payne M. J., 2011, MNRAS, 727, 74
- Zalamea I., Menou K., Beloborodov A. M., 2010, MNRAS, 409, L25